Synthesis and Characterization of Highly Efficient Near-Infrared Upconversion Sc 3+ /Er 3+ /Yb 3+ Tridoped NaYF 4

ARTICLE *in* THE JOURNAL OF PHYSICAL CHEMISTRY C · MARCH 2010

Impact Factor: 4.77 · DOI: 10.1021/jp908645h

4 AUTHORS, INCLUDING:

Qingming Huang
Fuzhou University
12 PUBLICATIONS **83** CITATIONS

Synthesis and Characterization of Highly Efficient Near-Infrared Upconversion $Sc^{3+}/Er^{3+}/Yb^{3+}$ Tridoped $NaYF_4$

Qingming Huang, Jianchang Yu,* En Ma, and Kaiming Lin

Instrumentation Analysis and Research Center, College of Materials Science and Engineering, Fuzhou University, Fuzhou, Fujian 350002, China

Received: September 7, 2009; Revised Manuscript Received: February 10, 2010

The blue, green, red, and UV upconversion (UC) emissions of hexagonal $NaYF_4$ were obviously enhanced by tridoping the structure with $Sc^{3+}/Er^{3+}/Yb^{3+}$. The effect of Sc^{3+} tridoping on the upconversion luminescence of $NaYF_4$: Er^{3+}/Yb^{3+} was investigated in detail. The blue, green, and red upconverted emissions corresponding to the excitation of infrared 980-nm light were remarkably enhanced and the decay time was obviously prolonged with different quantity Sc^{3+} tridoping. X-ray diffraction, X-ray photoelectron spectroscopy, and decay time investigations evidence that Sc^{3+} ions can tailor the local crystal field of the $NaYF_4$ host lattice, and the energy level $^4S_{3/2}$ was split. The UC emissive intensity mechanism was discussed based on XRD, XPS, and PL analysis data. This material is expected to be widely applied in biomedical, UC laser, solar energy, etc.

1. Introduction

In recent years, upconversion inorganic nanoparticles doped with trivalent rare-earth ions have attracted much attention[1−5] because of their superior spectroscopic properties. It can easily emite visible light under the excitation of near-infrared (NIR) diode lasers. It may lead to a great deal of potential application in many fields,[6−8] especially in biology, biomedicine,[9] catalyst,[10] and solar energy. At present researchers have focused their investigations on lanthanide-doped upconversion nanocrystals.[20] Hexagonal sodium yttrium fluoride ($NaYF_4$) is the most efficient host material for green, blue, and red upconversion phosphors to date. However, the application of $NaYF_4$:Er^{3+} is still very much constrained because of lower UC intensity. Many kinds of methods have been taken to enhance the UC intensity, such as annealed,[10,11] grain size reduction,[12−14] sensitizing agent codoped,[1,15] crystal surface coating,[8,16,17] and so on. Most of these methods have not achieved the desired results.

UC luminescence intensity is mainly dependent on electronic transition probabilities and self-specific absorption of UC emission. Auzel discussed upconversion and antistokes processes with f and d ions in solids.[21] Many investigations indicated Ln^{3+} ions were particularly sensitive to the surrounding environment.[18,22] A hypersensitive transition will be produced by changing the Ln^{3+} ions' environment. According to the formula of Judd−Ofelt the Ω_2 parameter is specially susceptive to the surroundings, which is caused by the change of local symmetry of rare earth ions. The crystal field effect will also be produced by the Ln^{3+} ions' surrounding change. For this reason we have an idea that one smaller trivalent ion (Sc^{3+}) can be tridoped in $NaYF_4$:Er^{3+}/Yb^{3+}, in order to change the local surrounding symmetry of rare earth ions, and enhance UC luminescence intensity.

Here we report on the crystal structure, UC luminescence, XPS of different quantity Sc^{3+} tridoped $NaYF_4$:Er^{3+}/Yb^{3+}. We have systematic experimental investigations in the Sc^{3+} ion effect on the UC intensity, radiation lifetime, electron binding energy of Ln^{3+} ions, and crystal structure (including bond distance and rare-earth ions' spacing).

* To whom correspondence should be addressed.

2. Experimental Section

Preparation. A sample of 3 mol % of Yb^{3+} and 2 mol % of Er^{3+} was selected for codoping in $NaYF_4$, and tridoping with the concentration of 0, 3, 5, 10, 15, or 20 mol % of Sc^{3+}. The rare-earth oxides RE_2O_3 (RE = Er,Yb) and Sc_2O_3 (99.999%) were purchased from Tianjin Feng-Etsu Chemical Co. All the other chemicals were purchased from Shanghai Schonborn Chemical Co. All chemicals are analytical grade reagents and are used directly without further purification. Trivalent nitrate stock solutions of 0.2 M were prepared by dissolving the corresponding metal oxide in concentrated nitric acid at elevated temperatures. In a typical procedure, a certain mole percentage of trivalent nitrate solutions was added into 20 mL of aqueous solution containing 0.4 mmol cosodium EDTA. After vigorous stirring for 30 min, 25 mL of an aqueous solution containing 0.2 mmol NaF and 0.3 mmol NH_4HF_2 was added into the above solution. The pH value of the solution was adjusted to 3.0 by the addition of 1 mol/L HF or 1 mol/L NaOH solution, with continuous stirring for 30 min. Then the emulsion mixture was moved to a PTFE-lined high-pressure pot and incubated in the oven at 195 °C for 48 h. After crystallization, the products were washed by deionized water and ethanol three times, respectively, and then dried in an oven at 60 °C.

Characterization. The elements Y/Yb/Er/Sc were analyzed by ICP Ultima2 of Jobin Yvon manufacture. X-ray powder diffraction (XRD) measurements were performed on a Panalytical X'pert Pro MPD diffractometer at a scanning rate of 1 deg/min in the 2θ range from 10° to 120°,with graphite monochromatized Cu Kα radiation (λ = 0.1540596 nm). Transmission electron microscopy (TEM) was performed with FEI Tecnai G2 F20 S-TWIN with a field emission gun operated at 200 kV. UC emission spectra were obtained with an Edinburgh instruments FSLP920 flourescence spectrophotometer by 980 nm OPTEK OPO LASER excitation. Absorption spectra of Yb^{3+} were measured by PE lambda 900 Spectrometer. All the measurements were performed with the same conditions and at room temperature.

10.1021/jp908645h
Published on Web 02/24/2010

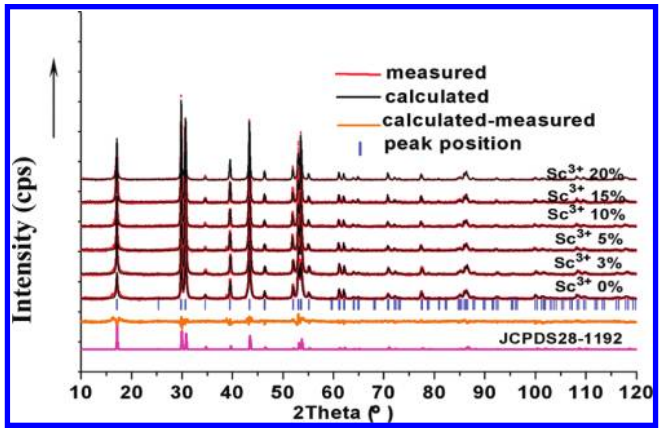

Figure 1. XRD curves of 0, 3, 5, 15, and 20 mol % Sc^{3+} tridoped samples (red lines), JCPDS 28-1192 curve (pink line), calculated XRD curve of each sample after crystal stucture refinement by Rietveld method (black lines). $Y_{obs}-Y_{cal}$ of Sc^{3+} 0 mol % tridoping sample (golden line), and bragg positions of 0 mol % Sc^{3+} tridoping sample (blue line).

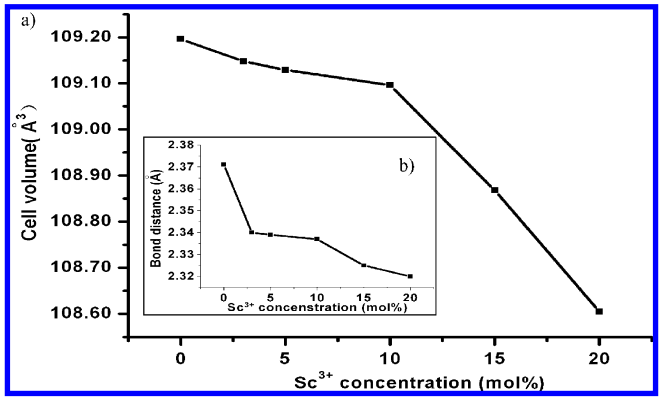

Figure 2. (a) Cell volumes of 0, 3, 5, 15, and 20 mol % Sc^{3+} tridoping samples; (b) average bond length of six samples.

3. Results and Discussion

Quantitative analysis results of the elements Y/Yb/Er/Sc are shown in Table 3 of the (Supporting Information), and the result is coherent with addition quantity. XRD characterizations of Sc^{3+} tridoped $NaYF_4$:Er^{3+}/Yb^{3+} are shown in Figure 1. XRD peak positions and intensities match closely with that of hexagonal β-$NaYF_4$ in JCPDS(28-1192). Different amounts of Sc^{3+} tridoping do not lead to other phase formation. XRD patterns (Figure 1) of the samples show well-defined peaks, indicating the synthesized Sc^{3+} tridoped $NaYF_4$:Er^{3+}/Yb^{3+} crystal is highly crystalline. The cell parameters and F^-−Ln^{3+} bonds of six samples were calculated by FullProf with crystal structure parameters of β-$NaYF_4$ and XRD curves of six samples. Each Ln^{3+} ion was linked with an F^- ion and the length of each bond was different. *R* values of crystal structure refinement are listed in Table 1 (Supporting Information), and all of them are smaller than 5. Cell volume and average value of bonds length are shown in Figure 2. The cell volume decreased with the rise of Sc^{3+} tridoping amount, and the change of the average Ln^{3+}−F^- bond length was the same with cell volume. This indicates that Sc^{3+} ions were doped in $NaYF_4$ lattice and lie in Y^{3+} positions because the radius of Sc^{3+}(74.5 pm) is smaller than that of Y^{3+}(90 pm), and it may be related to a change in symmetry that the cell volume of the $NaYF_4$ did not decrease linearly with increasing Sc^{3+} doping concentration.[23,24] TEM images of samples were shown in Figure 3. The shape of the grain is a uniform hexagonal short column, and its length and width are about 400 nm and 200 nm, respectively.

To investigate the influence of different Sc^{3+} tridoping concentrations on UC luminescence, the UC emission spectrum of six samples was measured with 980 nm Q-swith pulsed OPO laser excitation. The parameters of the excitation laser were pulse width 5 ns and repeat frequency 10 Hz, and the precise power density was 5 w/cm^2. All samples were measured under the same conditions. UC fluorescence was shown in Figure 4. Emissions were attributed to the following transitaions:$^4G_{11/2}$ to $^4I_{15/2}$ (~378 nm), $^2H_{9/2}$ to $^4I_{15/2}$ (~408 nm), $^2H_{11/2}$ to $^4I_{15/2}$ (~521 nm), $^4S_{3/2}$ to $^4I_{15/2}$ (~543 nm), $^4F_{9/2}$ to $^4I_{15/2}$ (~654 nm), $^4I_{9/2}$ to $^4I_{15/2}$ (~815 nm), and were shown in Figure 5. The UC luminescence intensity was changed obviously with the rising of Sc^{3+} tridoping concentration as Figure 4b. It shows that the intensity was weakened when 3 mol % Sc^{3+} was tridoped in, and then it was enhanced with the rising of Sc^{3+} tridoping concentration. When the Sc^{3+} tridoping concentration reached 10 mol %, the UC luminescence intensity reached its maximun and became more than five times that of the Sc^{3+} undoped sample. Then the intensity was weakened with the rise of the Sc^{3+} tridoping concentration. The changing trend of each emission was the same. The half-peak width of $^4S_{3/2}$ to $^4I_{15/2}$(~543 nm) emission was changed obviously, and the changing trend was the same with UC luminescence intensity change. This indicates the $^4S_{3/2}$ energy level and energy bandwidth had been influenced.

Figure 6a. depicts time evolution of the 521 nm emission of different Sc^{3+} tridoping concentration samples. The blue curve of Figure 6a shows three peaks clearly, indicating 521 nm emission was overlapped by three periods. UC emission decay time can be calculated by three group exponential functions and depicts decay time changing trends qualitatively. All curves can be well fitted with the following equation under the same right parameters' initial value.

$$I(t) = A + \mathrm{B1} * e^{-t/t1} + \mathrm{B2} * e^{-t/t2} + \mathrm{B3} * e^{-t/3t} + \mathrm{B4} * e^{-t/t4} + \mathrm{B5} * e^{-t/t5} + \mathrm{B6} * e^{-t/t6}$$

In this equation *A* and B1, B2, and B3 are all positive parameters indicating decay components, and B4, B5, and B6 are all negative parameters indicating rise components. The fitting results were given in Table 2 (Supporting Information). The decay time constants t1, t2, and t3 changed in the rang by 104.5−539.5, 12.8−102.5, and 3.1−39.4 μs, respectively; the rise time constants t4, t5, and t6 changed in the rang by 18.6−165.4, 7.5−52.8, and 5.2−37.2 μs, respectively. Parts b and c of Figure 6 depict the change tend of decay and rise time constants of different Sc^{3+} tridoping concentrations, indicating that rise and decay time can be tuned by tridoping different amounts of Sc^{3+} ion. When the tridoped concentration of Sc^{3+} was less than 3 mol %, the rise and decay time was decreased; if Sc^{3+} concentration was in the range of 5−10 mol %, the rise and decay time was extended; when the Sc^{3+} tridoping concentration was 10 mol %, the time constant was top; then the time constants decreased with the rise of Sc^{3+} tridoping concentration. Figure 7a depicts the decay time evolution of 543 nm emission of different Sc^{3+} concentration tridoping samples. The decay time evolution curves were divided into three parts clearly, and there are three peaks in each curve. This indicates emission of 543 nm consisted of three periods, and the interval of the three periods was changed with the changing of Sc^{3+} tirdoping concentration. When the Sc^{3+} tridoped concentration was in the range of 5−15 mol % their intervals were increased with the rise of Sc^{3+} concentration. When the Sc^{3+} concentration was more than 15 mol %, the interval was

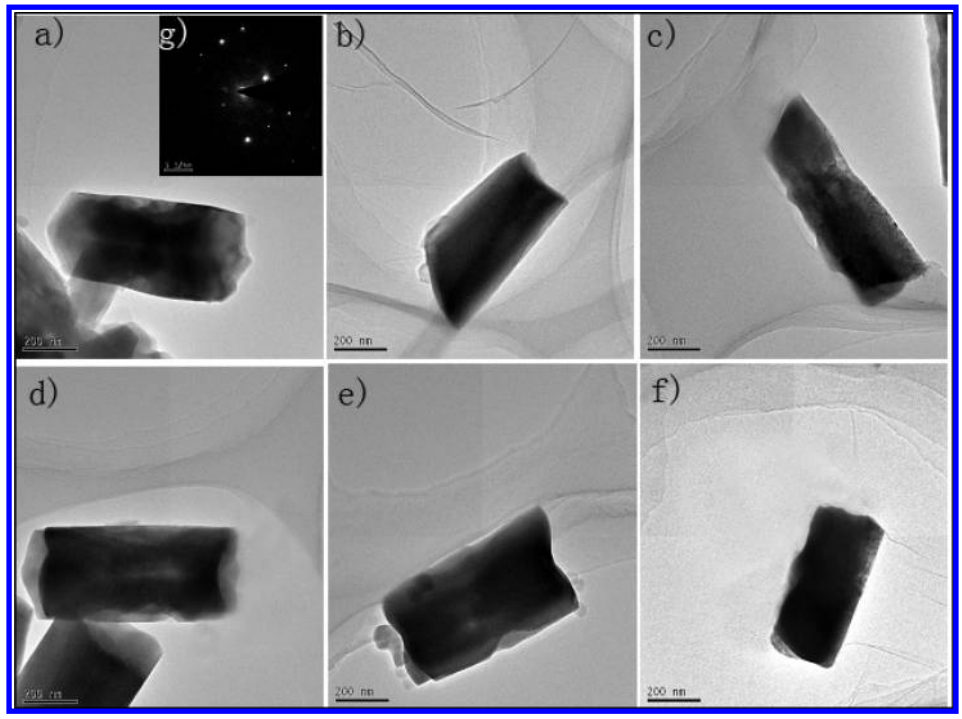

Figure 3. (a−f) TEM pictures of samples Sc 0%, Sc 3%, Sc 5%, Sc 10%, Sc 15%, and Sc 20%, respectively. (g) Diffraction pattern of panel a.

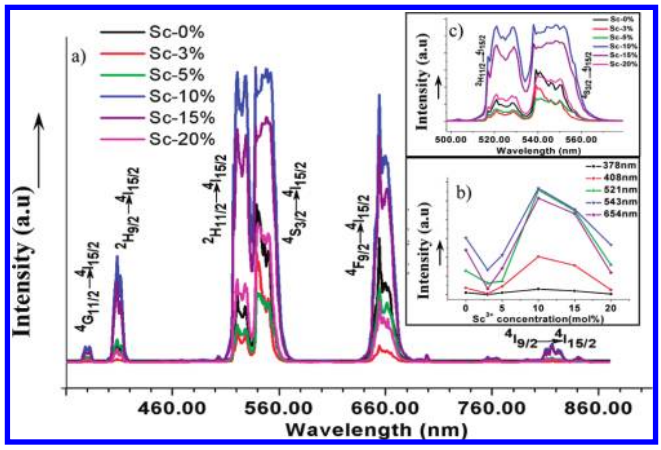

Figure 4. (a) UC emissions of $NaYF_4$: 2 mol % Er^{3+}/3 mol % Yb^{3+} tridoped with 0, 3, 5, 10, 15, and 20 mol % Sc^{3+}, respectively. (b) Intensity changing tend curves of 378, 409, 521, 539, and 654 nm emissions of different Sc^{3+} tridoping concentrations. (c) Partial enlargement of part a.

decreasd. When 10 or 15 mol % Sc^{3+} was tridoped the intervals were the most distinct. For furhter investigation of this decay time change, the Sliced TRES (time-resolved emission spectroscopy) method was adoped. TRES measurement of 521 and 543 nm UC emissions was shown in Figure 8. The decaying law of UC luminescence intensity coincides with decay time curves of Figures 6 and 7. The peaks profile of 543 nm emission of different Sc^{3+} tridoping concentrations is dissimilar, the left part of the 543 nm peak is higher than the right as shown in Figure 8a−c, and the profile has not changed with decay time increasing. But the left part of the 543 nm peak of 10/15 mol % Sc^{3+} tridoping samples is lower than the right, and it is changing with the decay time increasing. When the decay time is at 1.232 ms the profile of peak is reversed, the left part is higher than the right. There is a new peak at 538 nn that appeared in the curve of 10/15 mol % Sc^{3+} tridoping samples and disappeared at 1.232 ms. This indicates that the peak is a new energy level emission, and may be produced by $^2H_{11/2}$ or $^4S_{3/2}$ energy level split. For a further observation, the 543 nm peak moved to lower wavelength with decay time rise. These phenomena indicate that the energy levels of $^2H_{11/2}$ and $^4S_{3/2}$ have been split when 10/15 mol % Sc^{3+} ions were tridoped in, and the disciplinarian of electron transition has been altered.

Why did UC luminescence intensity and decay time change with different Sc^{3+} ion tridoping concentrations? They were possibly influenced by the changing of Er^{3+} surrounding ions and crystal field with different amounts of Sc^{3+} tridoping. This can be proved by an exact crystal structure. The crytal structure of each sample has been refined by FullProf.[25] Measurement and calculated XRD patterns were shown in Figure 1. After refinement the detailed structure parameters have been obtained, and then the bond length and the space between two trivalent cations can be calculated with crystal sructure parameters by Diamond software. The change tends of $F^-−Y^{3+}/Yb^{3+}/Er^{3+}/Sc^{3+}$ bond length and ion space between A and B were shown in Figures 9 and 10. The average lengths of r1 and r2 decreased with the rise of Sc^{3+} tridoping concentration in the rang of 0−10 mol %. When the Sc^{3+} tridoping concentration was rised higher than 10 mol % the average length of r1and r2 began to increase. The spaces between two trivalent cations of six samples were dissimilar with different Sc^{3+} tridoping concentrations. At first the space increased until 3 mol % Sc^{3+} was tridoped in. And then the space decreased with the rising of Sc^{3+} tridoping concentration. When the Sc^{3+} tridoping concentration was 10 mol %, the space reached the nadir of its value. Then further a rise in the Sc^{3+} concentration turned the space to increasing again. This fact has been confirmed by XPS analysis. Yb^{3+} and Er^{3+} binding energies were shown in Figures 11 and 12, respectively. Yb^{3+} and Er^{3+} binding energies went to their acmes when 10 mol % Sc^{3+} was tridoped in. The changing tend is opposite that of the bond length and the space between two trivalent cations is changed as mentioned above. So the results of crystal structure and binding energy analysis are accordant.

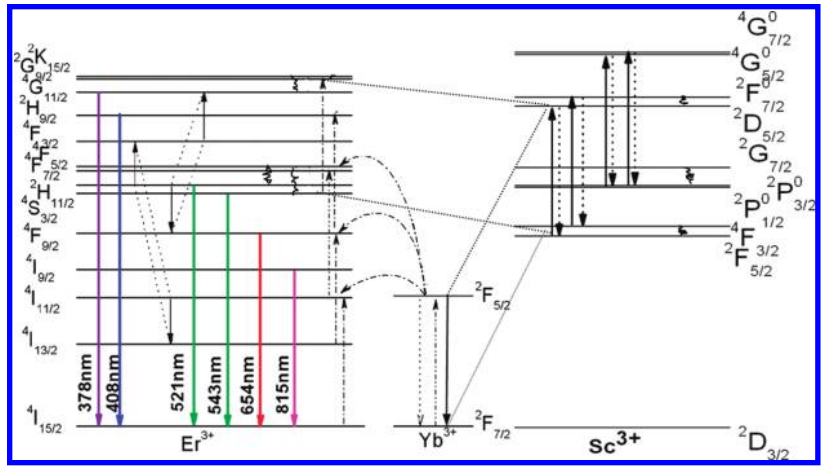

Figure 5. Schematic energy-level diagrams of the $Er^{3+}/Yb^{3+}/Sc^{3+}$ dopant ions and the mechanism after the sample was excited by 980 nm laser diode. The solid, dotted, and curly arrows indicate radiative, nonradiative energy transfer, and multiphoton relaxation processes, respectively. Two parallelograms indicate emission and absorption.

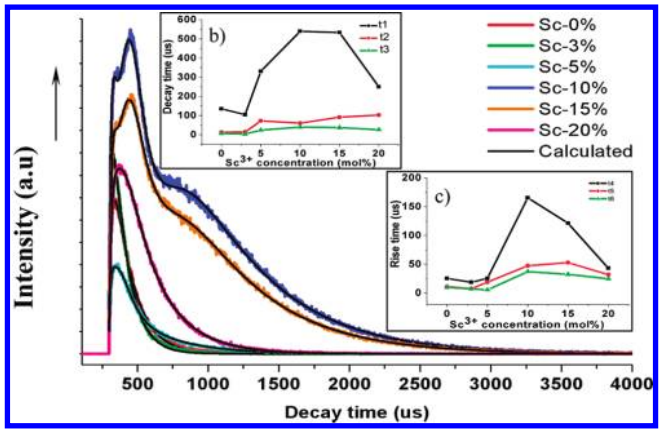

Figure 6. (a) Decay measured and calculated profiles of the $^2H_{11/2} \rightarrow {}^4I_{15/2}(Er^{3+} \sim 521$ nm) transition in $NaY_{0.95-x}Er_{0.02}Yb_{0.03}Sc_xF_4$ with x equal to 0, 0.03, 0.05, 0.10, 0.15, and 0.20. (b) Three decay lifetime constants changing tend of six samples. (c) Three rising time constants changing tend of six samples.

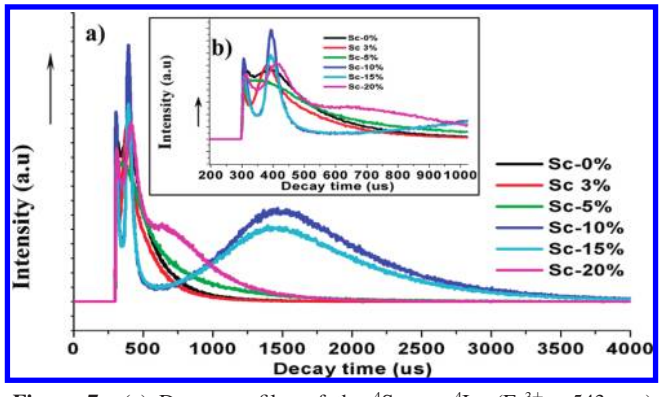

Figure 7. (a) Decay profiles of the $^4S_{3/2} \rightarrow {}^4I_{15/2}(Er^{3+} \sim 543$ nm) transition in $NaY_{0.95-x}Er_{0.02}Yb_{0.03}Sc_xF_4$ with x equal to 0, 0.03, 0.05, 0.10, 0.15, and 0.20. (b) Partial enlargement of part a.

What are reasons for the UC luminescence intensity enhancement? First, bond length and trivalent cation space were influenced by different Sc^{3+} tridoping concentrations. This indicates the surrounding environment of rare earth has been altered. The change of bond length, trivalent cation space, and rare-earth ions binding energy showed this. It also leads to an electron distribution density change. We can deduce the surrounding environment of the Sc^{3+} 10 mol % sample is the most asymmetric with the above crystal structure analysis results (the difference among r1, r2, and r3 is the largest). Asymmetric surrounding environment will lead to hypersensitive electron transition[26] and enhance UC luminescence intensity. Parts d and e of Figure 8 show a new UC emission at 538 nm that indicates the energy level was split, and the energy level positions rose or decreased so that the band gap would be reduced. For this reason the level gap between some energy levels of Er^{3+} was changed and can be exited by an incident 980 nm photon, promoting them to the $^2H_{11/2}$, $^4S_{3/2}$ level thus enhancing the population of th $^2H_{11/2}$, $^4S_{3/2}$ level. Second, cross-relaxation of energy between Er^{3+} and Sc^{3+} ions also enhanced the population of each emission level. And the internal quenching among Er^{3+}, Yb^{3+}, and Sc^{3+} ions was reduced by tridoping Sc^{3+} in $NaY_{0.95-x}Yb_{0.03}Er0_{0.02}Sc_xF_4$. Third, the efficiency of Yb^{3+} sensitization was enhanced when the right amount of Sc^{3+} was tridoped in, such as 10 mol %. The absorption spectrum of Yb^{3+} was shown in Figure 13. Sc 10%/Sc15% curves show a satellite peak at the left of 980 nm. This indicates the energy level gap of Yb^{3+} was altered and the ΔE could be compensated by absorbing or emitting phonons. The transition energy of the satellite peak may improve cross-relaxation with some energy level gap of Er^{3+} ions and then enhance the population of the emission energy level further. So UC luminescence intensity was certainly enhanced.

What are the reasons for the change of UC luminescence decay time? First, the electronic transition is very complex[19] in $NaY_{0.95-x}Yb_{0.03}Er0_{0.02}Sc_xF_4$. Auzel has discussed upconversion and antistokes processes of Er^{3+} in his paper.[21] Energy transfer of upconversion emission has several paths such as SET, CR, and CU. Each energy transfer course is very complex in this system. $^4S_{3/2}$, $^2H_{11/2}$ to $^4I_{15/2}$ emission of Er^{3+} ion is divided into two processes. At first the electron was excited to the $^4S_{3/2}$ and $^2H_{11/2}$ level from another lower level of Er^{3+} or relaxed to the $^4S_{3/2}$ and $^2H_{11/2}$ level from another higher energy level by the ESA, SET, CR, or CU path. Each electron experienced different courses especially in this rare-earth tridoping system. So the times for electrons to transfer to the $^4S_{3/2}$ and $^2H_{11/2}$ level were different. There are several channels for electrons to transfer to the $^4S_{3/2}$ and $^2H_{11/2}$ level. (a) The ground state electron of Er^{3+} absorbed an incident 980 nm photon energy and excited them to the $^4S_{3/2}$ or $^2H_{11/2}$ level, then relaxed to the ground state with 543 or 521 nm emission. (b) An incident 980 nm photon was strongly absorbed by Yb^{3+} ions and excited them to th $^2F_{5/2}$ level along with the direct absorption of Er^{3+} ions. Then the excited Yb^{3+} ions transferred their excitation energy to unexcited

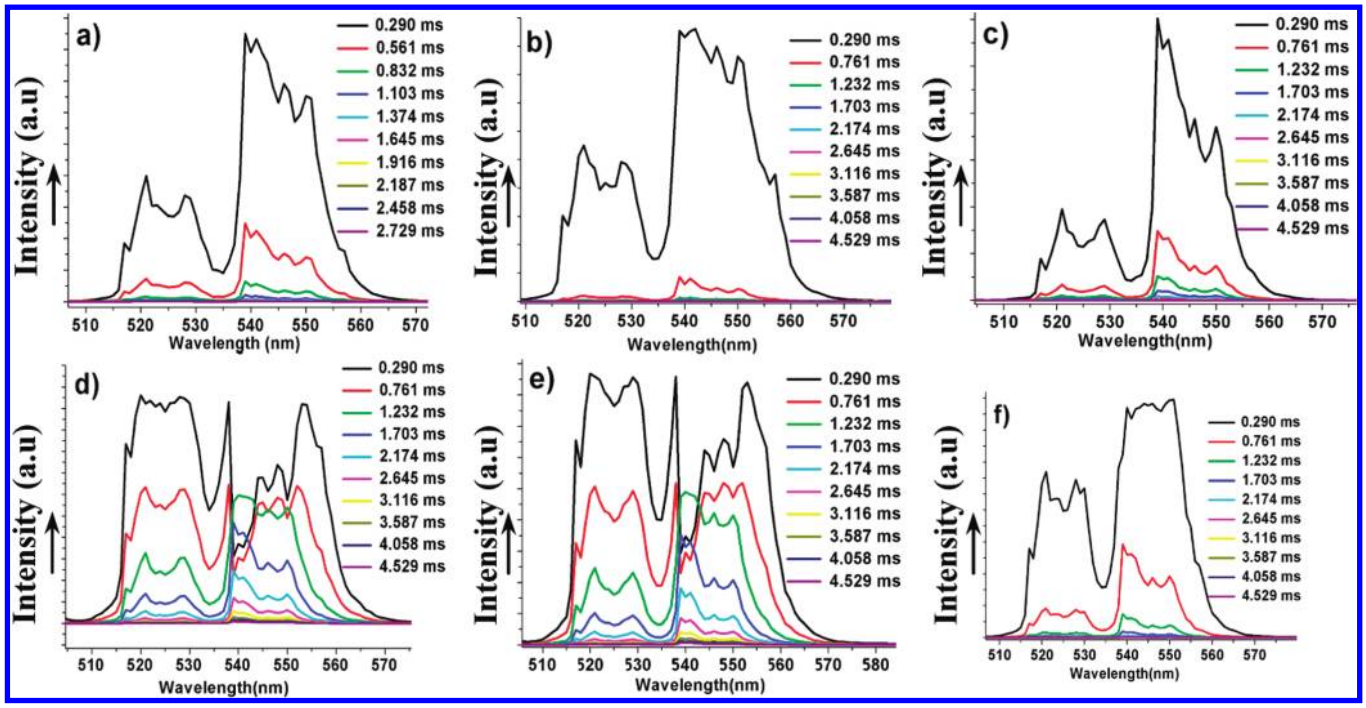

Figure 8. (a−f) Sliced TRES of 0, 3, 5, 10, 15, and 20 mol % Sc^{3+} tridoping samples, respectively.

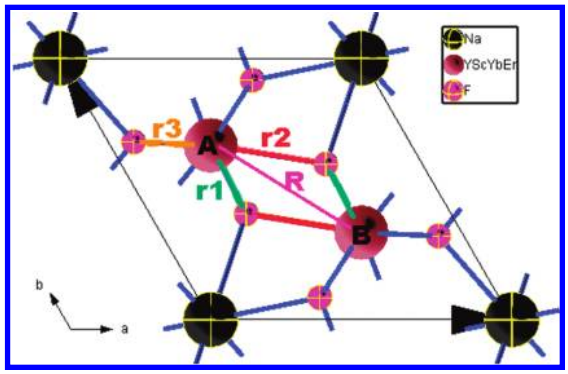

Figure 9. Crystal structure of $NaY_{0.95-x}Yb_{0.03}Er0_{0.02}Sc_xF_4$. r1, r2, and r3 denote three bonds between F^- and $Y^{3+}/Yb^{3+}/Er^{3+}/Sc^{3+}$. *R* denotes the space between A and B.

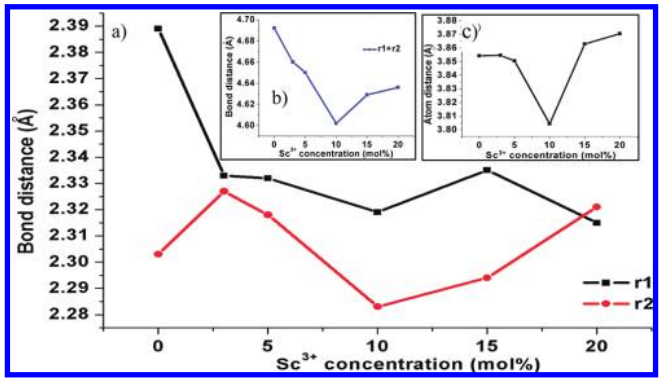

Figure 10. (a) Changing tend of the distance of bonds r1 and r2, (b) the sum of r1 and r2, and (c) the space between A and B atoms of different Sc^{3+} tridoping concentration samples, respectively.

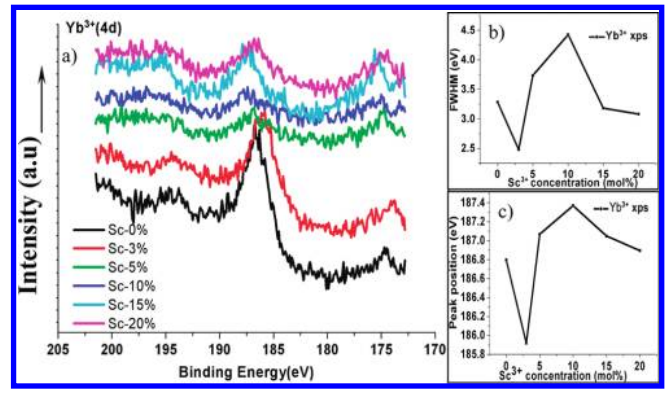

Figure 11. (a) XPS curves of Yb^{3+} with different Sc^{3+} concentrations; (b) half width of peaks; (c) peak position of different Sc^{3+} concentrations.

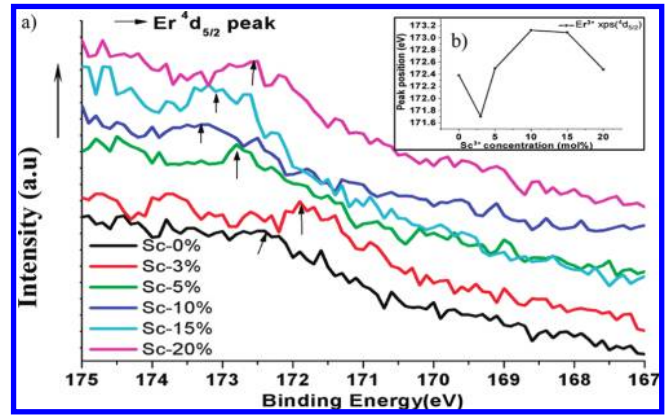

Figure 12. (a) XPS curves of Er^{3+} with different Sc^{3+} concentrations; (b) XPS peak positions of different Sc^{3+} concentrations.

Er^{3+} ions and excited them to the $^4S_{3/2}$ or $^2H_{11/2}$ level from the ground state. This course must be longer than course a. (c) Incident 980 nm photons or excited Yb^{3+} ions' excitation energy was absorbed by Sc^{3+} ions and excited them to a higher energy level. The excited Sc^{3+} ions transferred their relaxation energy to unexcited Er^{3+} ions and excited them to the $^4S_{3/2}$ or $^2H_{11/2}$ level. The excited Er^{3+} ions transferred their $^4G_{11/2}$ to $^2H_{11/2}$ relaxation energy to unexcited Sc^{3+} ions. Or cross-relaxation occurred between excited Er^{3+} ions and Sc^{3+} ions with absorption or emission of a phonon to compensate for the ΔE of energy gap. The time for this course is the longest, and this process is closely related to the amount of Sc tridoping. Three kinds of

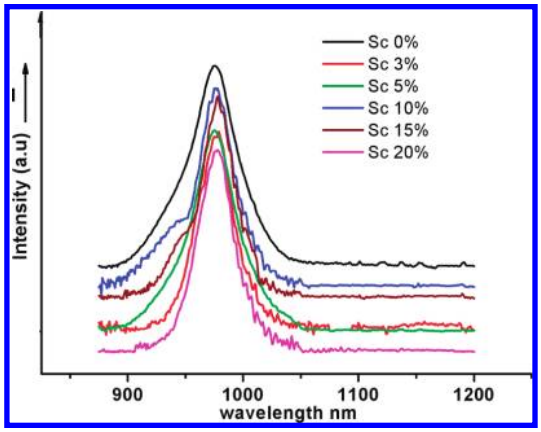

Figure 13. Yb^{3+} ion absorption spectra of different Sc^{3+} amounts of tridoping samples. The Sc 10% and Sc 15% curves show a satellite peak of 980 nm clearly.

energy transfer processes were shown in Figure 1 in the Supporting Information. The time for electrons staying on the energy level is the same in one material system, and the decay time depends on the time for electron transfer to the $^4S_{3/2}$ or $^2H_{11/2}$ level. In this work, the PL analysis results show different concentrations of Sc^{3+} tridoping strongly influenced the $^2H_{11/2}$ and $^4S_{3/2}$ level. This indicates the probability and the complexity of item c of the above discussion was altered by the change of Sc^{3+} tridoping concentration. So the emissions of 521 and 543 nm decay include three periods, and the decay time and the internal of three periods were changed with the changing of Sc^{3+} tridoping concentration. When Sc^{3+} tridoping concentration was 10 mol % the probability and the complexity of item c was the highest, the cross-relaxation course was the most complexed, and the time for electron to transfer to $^4S_{3/2}$ or $^2H_{11/2}$ was the longest. So the interval of three periods is the most clear, and the decay time is longest.

Potential Applications. First, this material can absorb near-infrared light at 980 nm and emit higher energy (378, 521, 543, and 654 nm) in an anti-Stokes process. If the emission intensity arrives at the application level, it can be applied in the solar energy field to extend the response range of solar energy.[27] And it can also be applied to the photocatalysis field, when this material combined with TiO_2 or other photocatalyst,[28] because catalytic performance will be enhanced by the UC process of the material. Second, it can be applied to the antifake field because the luminescence of this material can be excited by a 980 nm laser, which is invisible. Third, this material has excellent photostability, sharpness of fluorescence separation, and lower exiting energy, so it can be applied in biology, biomedicine, or imaging display.[29,30]

4. Conclusion

UC luminescence of $NaY_{0.95-x}Yb_{0.03}Er0_{0.02}Sc_xF_4$ was enhanced obviously by tridoping Sc^{3+} ions, which can be contrasted to the untridoped one, especially for higher energy emissions. XRD investigations illustrate that the bonds $F^- - Y^{3+}$ were changed and the local crystal field of $NaY_{0.95-x}Yb_{0.03}Er0_{0.02}Sc_xF_4$ host lattice can be expectedly tailored by substituting the Y^{3+} lattice sites with Sc^{3+} ions. Decay time analysis evidenced that 521 and 543 nm emissions were split into three periods and lifetimes were extended by Sc^{3+} ions tridoping. Therefore the Sc^{3+} tridoping method can be used for UC luminescence intensity enhancing or decay time tuning. The new emission of 538 nm can be produced by 10 or 15 mol % Sc^{3+} tridoping. We can obtain controllable UC intensity and tune decay time by tridoping diffirent amounts of Sc^{3+} in $NaYF_4$: Er^{3+}/Yb^{3+}. This material will have potential applications in the fields of optical display, photocatalysis, solar energy, biology, biomedicine, etc.

Acknowledgment. We are grateful to X.K.D. and X.H.Y. for support doing the TEM measurement and to R.Q.S. for support doing the absorption spectrum measurement.

Supporting Information Available: *R* values of crystal structure refinement by FullProf, rise, and Decay time constants of 521 nm Upconversion Emissions and ICP analysis results of $Y^{3+}/Yb^{3+}/Er^{3+}/Sc^{3+}$ of different Sc^{3+} concentration tridoping samples, as well as the energy transfer process for $Yb^{3+}/Er^{3+}/Sc^{3+}$:$NaYF_4$ (Figure 1). This material is available free of charge via the Internet at http://pubs.acs.org.

References and Notes

(1) Wang, F.; Liu, X. *J. Am. Chem. Soc.* **2008**, *130*, 5642–5643.
(2) Zeng, J. H.; Su, J.; Li, Z. H.; Yan, R. X.; Li, Y. D. *Adv. Mater.* **2005**, *17*, 2119–2123.
(3) Patra, A.; Saha, S.; Alencar, M. A. R. C.; Rakov, N.; Maciel, G. S. *Chem. Phys. Lett.* **2005**, *407*, 477–481.
(4) Zhang, X.; Liu, X.; Jouart, J. P.; Mary, G. *Chem. Phys. Lett.* **1998**, *287*, 659–662.
(5) Liang, L. F.; Wu, F.; Hu, H. L.; Wu, M. M.; Su, Q. *ChemInform* **2004**, 35.
(6) Wang, J.; Ma, T.; Zhang, G.; Zhang, Z.; Zhang, X.; Jiang, Y.; Zhao, G.; Zhang, P. *Catal. Commun.* **2007**, *8*, 607–611.
(7) Tero Soukka, T. R. K. K. *Ann. N.Y. Acad. Sci.* **2008**, *1130*, 188–200.
(8) Abdul Jalil, R.; Zhang, Y. *Biomaterials* **2008**, *29*, 4122–4128.
(9) Wang, M.; Liu, J. L.; Zhang, Y. X.; Hou, W.; Wu, X. L.; Xu, S. K. *Mater. Lett.* **2009**, *63*, 325–327.
(10) Wang, X.; Kong, X. G.; Yu, Y.; Sun, Y. J.; Zhang, H. *J. Phys. Chem. C* **2007**, *111*, 15119–15124.
(11) Wei, Y.; Lu, F.; Zhang, X.; Chen, D. *J. Alloys Compd.* **2007**, *427*, 333–340.
(12) Vetrone, F.; Boyer, J. C.; Capobianco, J. A. *J. Phys. Chem. B* **2002**, *106*, 5622–5628.
(13) Vetrone, F.; Boyer, J. C.; Capobianco, J. A.; Speghini, A.; Bettinelli, M. *Chem. Mater.* **2003**, *15*, 2737–2743.
(14) Capobianco, J. A.; Boyer, J. C.; Vetrone, F.; Speghini, A.; Bettinelli, M. *Chem. Mater.* **2002**, *14*, 2915–2921.
(15) Vetrone, F.; Boyer, J. C.; Capobianco, J. A.; Speghini, A.; Bettinelli, M. *J. Phys. Chem. B* **2003**, *107*, 1107–1112.
(16) Li, Z. Q.; Zhang, Y. *Angew. Chem.* **2006**, *118*, 7896–7899.
(17) Yan, W.; Weiping, Q.; Jisen, Z.; Chunyan, C.; Jishuang, Z.; Ye, J. *J. Rare Earth* **2007**, *25*, 605–608.
(18) Chen, G.; Liu, H.; Liang, H.; Somesfalean, G.; Zhang, Z. *J. Phys. Chem. C* **2008**, *112*, 12030–12036.
(19) Inokuti, M.; Hirayama, F. *J. Chem. Phys.* **1965**, *43*, 1978.
(20) Wang, F.; Liu, X *Chem. Soc. Rev.* **2009**, *38*, 976.
(21) Auzel, F. *Chem. Rev.* **2004**, *104*, 139–174.
(22) Sommerdijk, J. L. *J. Lumin.* **1973**, *6*, 61.
(23) Baikie, T.; Ng, G. M. H.; Madhavi, S.; Stevin, S.; Pramana; Blake, K.; Elcombec, M.; Whitea, T. J. *J. Dalton Trans.* **2009**, 6722.
(24) King, H. W. *J. Mater. Sci.* **1966**, *1*, 79.
(25) Krämer, K.W.; Biner, D.; Frei, G.; Gudel, H. U.; Hehlen, M. P.; Luthi, S. R. *Chem. Mater.* **2004**, *16*, 1244.
(26) Huang, T.; Hsieh, W. *J. Fluoresc.* **2009**, *19*, 511.
(27) Ahrens, B.; Loper, P.; Goldschmidt, C. J.; Gluna, S.; Henke, B.; Miclea, P. T.; Schweizer, S. *Phys. Status Solidi A* **2008**, *205*, 2822–2830.
(28) Wang, J.; Zhang, G.; Zhang, Z.; Zhang, X.; Zhao, G.; Wen, F.; Pan, Z.; Li, Y.; Zhang, P.; Kang, P. *Water Res.* **2006**, *40*, 2143–2150.
(29) Abdul Jalil, R.; Zhang, Y. *Biomaterials* **2008**, *29*, 4122–4128.
(30) Wei, Y.; Lu, F.; Zhang, X.; Chen, D. *J. Alloys Compd.* **2007**, *427*, 333–340.

JP908645H